# THE DUAL ROLE OF MITOCHONDRIAL SUPEROXIDE IN ARSENITE TOXICITY: signaling at the boundary between apoptotic commitment and cytoprotection

Mara Fiorani, Andrea Guidarelli, Valentina Capellacci, Liana Cerioni, Rita Crinelli and Orazio Cantoni*

*Dipartimento di Scienze Biomolecolari, Università degli Studi di Urbino "Carlo Bo", 61029 Urbino, Italy*

Author Email addresses:

mara.fiorani@uniurb.it; andrea.guidarelli@uniurb.it; valentina.capellacci@uniurb.it; liana.cerioni@uniurb; rita.crinelli@uniurb.it; orazio.cantoni@uniurb.it

*Corresponding author: Prof. Orazio Cantoni, Dipartimento di Scienze Biomolecolari, Sezione di Farmacologia e Farmacognosia, Università degli Studi di Urbino, Via S. Chiara 27, 61029 Urbino (PU), Italy. Tel: +39-0722-303523; Fax: +39-0722-303521; e-mail: orazio.cantoni@uniurb.it

**Abbreviations:** AA, L-ascorbic acid**;** BSO, DL-buthionine-[S,R]-sulfoximine**;** CsA, cyclosporin A; DHR, dihydrorhodamine 123; DTNB, dithiobis-(2-nitrobenzoic acid); EB, extracellular buffer; γ-GCS, γ-glutamylcysteine synthase; GCLC, γ-GCS catalytic heavy subunit; GCLM, γ-GCS regulatory light subunit; GSH, glutathione; Keap1, Kelch-like ECH-associated protein 1; Mito$O_2^{\cdot-}$, mitochondrial superoxide; MPT, mitochondrial

permeability transition; NO, nitric oxide; Nrf2, nuclear factor erythroid 2 p45-related factor 2; $O_2^{\cdot -}$, superoxide; PBS, phosphate buffered solution; RD cells, respiration-deficient cells.


## Abstract

Arsenite toxicity is in numerous cellular systems dependent on the formation of reactive oxygen and or nitrogen species. This is also true in U937 cells in which the metalloid selectively promotes the formation of mitochondrial superoxide (mito$O_2^{\cdot -}$) rapidly converted to diffusible $H_2O_2$. We tested the hypothesis that, under the same conditions, mito$O_2^{\cdot -}$ also mediates the triggering of a parallel survival signaling. We found that a low concentration of the metalloid causes an early activation of nuclear factor erythroid 2 p45-related factor 2 (Nrf2), and a downstream signaling leading to enhanced GSH biosynthesis, *via* a mechanism sensitive to various treatments/strategies selectively preventing mito$O_2^{\cdot -}$ formation. Under the same conditions, the toxic effects mediated by arsenite, leading to delayed mitochondrial permeability transition (MPT)-dependent apoptosis, were also prevented. Additional studies revealed remarkable similarities in the kinetics of mito$O_2^{\cdot -}$ formation, MPT induction, Nrf2 activation and GSH biosynthesis, prior to the onset of apoptosis in a small portion of the cells. Importantly, mito$O_2^{\cdot -}$ formation, as well as the ensuing toxic events, were significantly potentiated and anticipated under conditions associated with inhibition of *de novo* GSH biosynthesis triggered by the metalloid through Nrf2 activation.

We conclude that, in the arsenite toxicity paradigm under investigation, mito$O_2^{\cdot -}$ represents the only trigger of two opposite pathways leading to activation of the Nrf2 signaling and/or to a MPT-dependent apoptotic death. The first pathway, through enhanced GSH biosynthesis, mitigates the extent of further mito$O_2^{\cdot -}$ formation, thereby limiting and delaying an otherwise rapid and massive apoptotic death.

**Keywords:** arsenite; mitochondrial superoxide; Nrf2, GSH; mitochondrial permeability transition; apoptosis

## 1. Introduction

Arsenite is a widely diffused environmental toxicant. Epidemiological studies have demonstrated that human exposure to the metalloid, mainly resulting from the ingestion of contaminated drinking water, significantly increases the risk to develop various types of cancer and other chronic pathologies (Flora, 2011; Jomova et al., 2011). Although various mechanisms have been thus far proposed to explain the carcinogenic and toxic effects of the metalloid, in particular those resulting from its direct binding to thiol residues of target molecules (Shen et al., 2013; Watanabe and Hirano, 2013; Mandal, 2017), the involvement of reactive oxygen species (ROS) in these events is nowadays widely accepted (Flora, 2011; Jomova et al., 2011; Ellinsworth, 2015). Indeed, numerous studies have used various approaches to provide an indication of ROS formation and to infer the involvement of these species in the resulting lesions through the demonstration of a protective effect mediated by antioxidant supplementation (Flora, 2011; Jomova et al., 2011; Rao et al., 2017).

Less studies have instead addressed the question of the origin and identity of the ROS produced in response to arsenite, and the limited amount of information available indicates that the mechanism(s) leading to superoxide ($O_2^{-\cdot}$) formation is largely dependent on the cell type and treatment condition. For example, the involvement of NADPH oxidase has been reported in some cell types (Smith et al., 2001; Straub et al., 2008; Flora, 2011; Li et al., 2014; Ellinsworth, 2015), in which the relevance of this pathway of $O_2^{-\cdot}$ production is likely dependent on the level of expression of NADPH oxidase itself. Activation of this pathway may then result in mitochondrial dysfunction, thereby recruiting an additional mechanism of $O_2^{-\cdot}$ formation (Li et al., 2014). In this perspective, the selective activation of mitochondrial $O_2^{-\cdot}$ ($mitoO_2^{-\cdot}$) formation is more likely to take place in cell types poorly expressing NADPH oxidase. Evidence

of mito$O_2^{-\cdot}$ formation has been provided in a limited number of studies (Flora, 2011; Jomova et al., 2011; Guidarelli et al., 2016a; Guidarelli et al., 2016b). Additional factors affecting the cell type-dependence of the ROS response to arsenite are related to the expression of nitric oxide (NO) synthase, as the diffusion-limited reaction of $O_2^{-\cdot}$ with NO leads to the formation of peroxynitrite, a highly reactive and toxic species (Liu et al., 2005; Jomova et al., 2011; Ellinsworth, 2015). Cells not expressing NO synthase will be eventually damaged by $H_2O_2$, the dismutation product of $O_2^{-\cdot}$, with different sub-cellular concentrations of the oxidant expected to result from mito$O_2^{-\cdot}$ formation, associated with the effect of manganese superoxide dismutase, or NADPH-oxidase-derived $O_2^{-\cdot}$, associated with the action of cupper/zinc superoxide dismutase.

These simple considerations, while representing only a small part of a more complicate scenario, nevertheless emphasize the importance of learning more on the site in which ROS are being generated in response to arsenite. These mechanisms necessarily impact on the identity, and sub-cellular concentrations, of the downstream species produced and are also critical to correctly address the study of the indirect effects of arsenite, for example at the level of gene expression, induction of damage on different sub-cellular targets, apoptotic and even survival signaling responses.

By keeping these considerations in mind, we initially characterized the effects of arsenite in promonocytic U937 cells to understand more on the antileukemic and toxic effects of the metalloid (Guidarelli et al., 2015; Guidarelli et al., 2016a). Our interest was also stimulated by the observation that in these cells low concentrations of arsenite (e.g., 2.5 μM) selectively promote mito$O_2^{-\cdot}$ formation, in the absence of detectable effects mediated by NADPH oxidase (Guidarelli et al., 2016b). This notion was established using various approaches and significantly greater concentrations of the metalloid were necessary in order to promote detectable NADPH oxidase activation. As an example, 10 μM arsenite caused in respiration-deficient U937 cells (which fail to produce mito$O_2^{-\cdot}$ in response to 2.5 μM arsenite) a NADPH

oxidase inhibitor-sensitive DHR fluorescence response similar to that mediated by 2.5 μM arsenite in respiration-proficient cells.

Thus, the metalloid caused the selective formation of mito$O_2^{-\cdot}$ and we were indeed able to selectively suppress this response with rotenone, an inhibitor of complex I (Degli Esposti, 1998), or using the same cells manipulated to induce respiratory deficiency (Guidarelli et al., 2016a; Guidarelli et al., 2016b). It is important to remind that U937 cells are highly glycolytic, and therefore maintain high ATP levels, and remain viable, under conditions of impaired function/activity of the mitochondrial respiratory chain (Brand and Hermfisse, 1997).

An additional advantage of the specific cell type employed is related to the expression of high affinity transporters of L-ascorbic acid (AA) in both the plasma and mitochondrial membranes (Azzolini et al., 2013; Fiorani et al., 2015a; Fiorani et al., 2015b), a condition favoring the selective accumulation of AA in mitochondria after exposure to low extracellular concentrations of the vitamin (Azzolini et al., 2013; Fiorani et al., 2015a). Under these conditions, intramitochondrial AA very rapidly and effectively scavenged mito$O_2^{-\cdot}$ (Guidarelli et al., 2016a). Using these treatments, we were able to demonstrate a selective suppression of ROS formation mediated by arsenite, and hence establish the pivotal role of mito$O_2^{-\cdot}$ and its down-stream products in the induction of the deleterious effects elicited by the metalloid (Guidarelli et al., 2017).

The specific characteristics of the U937 cell clone used in our laboratory can also be used to address additional questions, for example related to the role of mito$O_2^{-\cdot}$ in the activation of specific cytoprotective signaling pathways, as the one connected to the nuclear factor (erythroid-2 related) factor 2 (Nrf2) (Abdul-Aziz et al., 2015; Tebay et al., 2015; Hourihan et al., 2016).

Oxidative and electrophilic stress are associated with an initial dissociation of Nrf2 from Kelch-like ECH-associated protein 1 (Keap1) and its subsequent translocation and accumulation in the nucleus (Tebay et al., 2015; Hourihan et al., 2016). The transcription factor promotes enhanced expression of an array of antioxidant enzymes (Abdul-Aziz et al., 2015; Tebay et al.,

2015; Hourihan et al., 2016), which include γ-glutamylcysteine synthase (γ-GCS, (Abdul-Aziz et al., 2015; Tebay et al., 2015)), the rate-limiting enzyme of GSH biosynthesis (Griffith and Mulcahy, 1999; Franklin et al., 2009), comprising a catalytic heavy subunit, (GCLC) and a regulatory light subunit (GCLM). Activation of these pathways leading to enhanced GSH biosynthesis is of extreme importance for providing cytoprotection in a variety of toxicity paradigms (Flora, 2011; Hou et al., 2014; Forman, 2016).

It has been reported that arsenite induces the dissociation of Nrf2 from Keap 1 (Pi et al., 2003; Lau et al., 2013). Although some studies claimed a role for a direct binding of arsenite to either Keap 1 or Nrf2 (He and Ma, 2009; He and Ma, 2010), Nrf2 activation is often reported to depend also on ROS formation. This notion is normally established by studies showing that Nrf2 activation is sensitive to very high concentrations of N-acetylcysteine (Ray et al., 2015; Rossler and Thiel, 2017), or other antioxidants (Choudhury et al., 2016; Gong et al., 2016), with a need of a more selective approach linking the cytoprotective signaling to the specific sources from which ROS are released by the metalloid.

The study of the effect of mito$O_2^{\cdot-}$ in the Nrf2 signaling, using selective strategies to prevent the formation of these species, would therefore allow a more clear definition of their role in Nrf2 activation. The approach of selectively targeting mito$O_2^{\cdot-}$ to understand its role in a cytoprotective signaling appears even more important under conditions in which the same species is also involved in the triggering of events leading to apoptosis.

In this perspective, the respective timing of these responses appears of particular importance to determine the dynamics regulating critical steps of the final decision of the cells to survive or die. This information is necessary to further our knowledge, thus far limited to the demonstration that cells overexpressing Nrf2 (or downstream effectors) are particularly resistant to arsenite, and that down-regulation of these systems remarkably enhances the sensitivity of the cells to the metalloid (Wang et al., 2007; Jiang et al., 2009; Yang et al., 2012; Son et al., 2015; Chen et al., 2017).

156 The present study was designed to determine the role of mito$O_2^{-\cdot}$ released in response to a
157 low concentration (i.e., promoting delayed apoptosis in a limited portion of cells) of arsenite in
158 the induction/activation of Nrf2 (Pi et al., 2003; Li et al., 2013). Our results indicate that
159 mito$O_2^{-\cdot}$ is responsible for the induction of two opposite pathways associated with the early
160 activation of the Nrf2 signaling and the delayed induction of mitochondrial permeability-
161 transition (MPT)-dependent apoptosis. The first pathway significantly blunted and delayed the
162 MPT-dependent apoptosis induced by the metalloid through a mechanism associated with
163 enhanced GSH biosynthesis and inhibition of excessive mito$O_2^{-\cdot}$ formation.
164

## 2. Materials and Methods

### *2.1. Chemicals.*

Sodium arsenite, AA, rotenone, diphenyleneiodonium (DPI), apocynin (Apo), phorbol-12-myristate-13-acetate (PMA), DL-buthionine-[S,R]-sulfoximine (BSO), Hoechst 33342, GSH, dithiobis-(2-nitrobenzoic acid), (DTNB) as well most of the reagent-grade chemicals were purchased from Sigma-Aldrich (Milan, Italy). Cyclosporin A (CsA) was from Novartis (Bern, Switzerland). Dihydrorhodamine 123 (DHR) and MitoTracker Red CMXRos were purchased from Molecular Probes (Leiden, The Netherlands). Acetonitrile was acquired from Carlo Erba (Carlo Erba Reagenti, Milan, Italy).

### *2.2. Cell culture and treatment conditions.*

U937 human myeloid leukemia cells were cultured in suspension in RPMI 1640 medium (Sigma-Aldrich, Milan, Italy) supplemented with 10% fetal bovine serum (Euroclone, Celbio Biotecnologie, Milan, Italy), penicillin (100 units/ml) and streptomycin (100 µg/ml) (Euroclone), at 37 °C in T-75 tissue culture flasks (Corning Inc., Corning, NY, USA) gassed with an atmosphere of 95% air-5% $CO_2$. U937 cells were made respiration-deficient (RD cells) as indicated in (Guidarelli et al., 2016b). Sodium arsenite was prepared as a 1 mM stock solution in saline A (140 mM NaCl, 5 mM KCl, 4 mM $NaHCO_3$, and 5 mM glucose; pH 7.4) and stored at 4°C. Cells (1 x $10^5$ cells/ml) were exposed to arsenite in complete RPMI 1640 culture medium, as reported in the legends to the figures. A 10 mM AA stock solution was prepared in extracellular buffer (EB, 15 mM Hepes, 135 mM NaCl, 5 mM KCl, 1.8 mM $CaCl_2$, 0.8 mM $MgCl_2$, pH 7.4) immediately before use. Cells (1 x $10^6$ cells/ml) were treated with AA in EB supplemented with 0.1 mM dithiothreitol for 15 min at 37°C. Stability of AA under these conditions was assessed by monitoring the absorbance at 267 nm for 15 min ($\varepsilon_{267}$ =14,600 $M^{-1}cm^{-1}$).

### *2.3. Western Immunoblotting analysis.*

After treatments, the cells were washed with phosphate buffer saline (PBS, 136 mM NaCl, 10 mM $Na_2HPO_4$, 1.5 mM $KH_2PO_4$, 3 mM KCl; pH 7.4) and lysed by sonication in a sodium dodecyl

sulphate (SDS) buffer containing 50 mM Tris-HCl pH 8.0, 2% (w/v) SDS, 10 mM N-ethylmaleimide, supplemented with a commercial cocktail of protease inhibitors (Roche Diagnostic, Monza, Italy). Lysates were boiled for 3 min and then centrifuged for 5 min at 12000 x g. The protein content was determined according to Lowry (Lowry et al., 1951), using bovine albumin as standard. Proteins were separated on 8% SDS polyacrylamide gels, transferred onto nitrocellulose membrane and probed with the following antibodies: anti Nrf2 (D1Z9C, Cell Signaling Technology, Leiden, The Netherlands), anti GCLC (PA5-16581, ThermoFisher Scientific, Monza, Italy) and anti actin (A2066, Sigma-Aldrich). Immunoreactive bands were detected using horseradish peroxidase-conjugated secondary antibody (BioRad, Milan, Italy). Peroxidase activity was detected with the enhanced chemiluminescence detection method (WesternBright ECL, Advasta, Roma, Italy).

*2.4. Measurement of total, protein and non-protein thiols.*

Total, protein and non-protein thiols were colorimetrically quantified by DTNB (Ellman, 1959). After treatments, the cells (4 x $10^6$) were washed three times with PBS and the pellets resulting from the last centrifugation were suspended in lysis buffer (0.1% Triton X-100, 0.1 M, $Na_2HPO_4$, 5 mM EDTA, pH 7.5) and incubated for 10 min at ice-bath temperature. The total thiol content was measured spectrophotometrically, at 412 nm, using DTNB ($\varepsilon_{412}$ = 13,600 $M^{-1} \cdot cm^{-1}$). For the assessment of protein thiols, the lysates were centrifuged on 10,000 MWCO centrifugal filters AMICON® ULTRA 4 (Millipore, Milan, Italy) and the concentrated protein (with molecular weight ≥ 10 kDa) fractions were analyzed as indicated above. Non-protein thiol content was determined in the acid soluble fraction obtained from the same lysates, as described by Beutler (Beutler, 1984).

*2.5. Measurement of GSH content by High Performance Liquid Chromatography.*

The cells (1x$10^6$) were suspended in 100 µl of lysis buffer, vortexed and kept for 10 min on an ice bath. Thereafter, 15 µl of 0.1 N HCl and 140 µl of precipitating solution (0.2 M–glacial meta-phosphoric acid, 5 mM sodium EDTA, 5 M NaCl) were added to the samples. After

centrifugation, the supernatants were collected and kept at –20° C until the HPLC analyses. Just before analysis, 60 $\mu$l of the acid extract were supplemented with 15 $\mu$l of 0.3 M $Na_2HPO_4$ and 15 $\mu$l of a solution containing 20 mg of DTNB in 100 ml of sodium citrate (1% w/v). The mixture was stirred for 1 min at room temperature and, after 5 min, filtered through 0.22 μm pore micro-filters. The resulting samples were finally analyzed for their GSH content by an HPLC assay (Brundu et al., 2016), using a 15 cm x 4.6 mm, 5 μm Supelco Discovery® C18 column (Supelco, Bellefonte, PA). The UV absorption was detected at 330 nm. The injection volume was 20 μl. The retention time of GSH was approximately 15.7 min.

*2.6. DHR fluorescence assay.*

The cells were incubated for 30 min with 10 μM DHR prior to the end of the incubation with arsenite, washed three times and analysed with a fluorescence microscope. Fluorescence images were captured with a BX-51 microscope (Olympus, Milan, Italy), equipped with a SPOT-RT camera unit (Diagnostic Instruments, Delta Sistemi, Rome, Italy) using an Olympus LCAch 40 x/0.55 objective lens. The excitation and emission wavelengths were 488 and 515 nm with a 5-nm slit width for both emission and excitation. Images were collected with exposure times of 100-400 ms, digitally acquired and processed for fluorescence determination at the single cell level on a personal computer using J-Image software. Mean fluorescence values were determined by averaging the fluorescence values of at least 50 cells/treatment condition/experiment.

*2.7. Measurement of mitochondrial membrane potential.*

The cells were incubated for 30 min with 50 nM MitoTracker Red CMXRos prior to the end of the incubation with arsenite, washed three times and analyzed with a fluorescence microscope. The resulting images were taken and processed as described above. The excitation and emission wavelengths were 545 and 610 nm, respectively, with a 5-nm slit width for both emission and excitation. Mean fluorescence values were determined by averaging the fluorescence values of at least 50 cells/treatment condition/experiment.

*2.8. Immunofluorescence analysis.*

After treatments, the cells were suspended in 2 ml of saline A and incubated for 30 min in 35-mm tissue culture dishes containing an uncoated coverslip. Under these conditions, cells rapidly attach to the coverslip. In some experiments the cells were incubated for 5 min with the cell-permeable DNA dye (Hoechst 33342, 10 μM) prior to the end of incubation to stain the nucleus. The cells were then fixed for 1 min with 95% ethanol/5% acetic acid, washed with PBS and blocked in PBS containing bovine serum albumin (2% w/v) (30 min at room temperature). The cells were subsequently incubated with rabbit polyclonal anti-$P47^{phox}$ (sc-17844) (1:100 in PBS supplemented with 2% bovine serum albumin; Santa Cruz Biotechnology Inc. USA), rabbit polyclonal anti-Nrf2 (1:50 in PBS containing 2% bovine serum albumin; Santa Cruz Biotechnology) or monoclonal anti-cytochrome c antibody (1:100 in PBS containing 2% bovine serum albumin; Santa Cruz Biotechnology) stored for 18 h at 4° C, washed and then incubated for 3 h in the dark with fluorescein isothiocyanate (Santa Cruz Biotechnology)-conjugated secondary antibody diluted 1:100 in PBS. Stained cells were captured with a fluorescence microscope and the resulting images were processed for fluorescence determination as described above.

*2.9. Fluorogenic caspase 3 assay.*

Caspase 3-like activity was monitored as described in Guidarelli *et al.* (Guidarelli et al., 2005). Briefly, the cells were lysed and aliquots of the extract (30 μg proteins) were incubated with 12 μM Ac-DEVD-AMC, at 30 °C. Caspase 3-like activity was determined fluorometrically, with excitation at 360 nm and emission at 460 nm, by quantifying the release of aminomethylcoumarin (AMC) from cleaved caspase 3 substrate (Ac-DEVD-AMC).

*2.10. Analysis of apoptosis with the Hoechst 33342 assay.*

After treatments, the cells were incubated for 5 min with 10 μM Hoechst 33342 and then analysed with a fluorescence microscope to assess their nuclear morphology (chromatin condensation and fragmentation). Cells with homogeneously stained nuclei were considered viable.

*2.11. Statistical analysis.*

269 The results are expressed as means ± SD. Statistical differences were analyzed by one-way
270 ANOVA followed by Dunnett's test for multiple comparison or two-way ANOVA followed by
271 Bonferroni's test for multiple comparison. A value of $P < 0.05$ was considered significant.
272

## 3. Results

### *3.1. Time-dependence of the activation of the Nrf2 signalling pathway.*

Logarithmically growing U937 cells were exposed for increasing time intervals to 2.5 μM arsenite and then processed for Western blot analysis of Nrf2 protein expression. As shown in Fig. 1A, very low levels of Nrf2 were detected in whole lysates from untreated cells during the 16 h of incubation. Expression of the transcription factor was instead remarkably enhanced in cells exposed for 4 h to arsenite, with a progressive decline being observed al later times of incubation. Enhanced Nrf2 expression is normally associated with its nuclear translocation and the ensuing transactivation of target genes (Abdul-Aziz et al., 2015; Tebay et al., 2015; Hourihan et al., 2016). Consistently, immunofluorescence studies provided evidence of Nrf2 nuclear translocation after a 6 h exposure to arsenite (Fig. 1B). In addition, expression of GCLC was significantly increased 4 h after addition of arsenite. The maximal increase in GCLC expression was detected at 6 h and these levels were maintained throughout the entire period of exposure to the metalloid. These results are indicative of a positive effect of arsenite on GSH biosynthesis. A significant increase in cellular GSH content was indeed detected in cells exposed for 4 h to the metalloid, with a plateau reached at the 8 h time point (Fig. 1C).

A final set of experiments was performed in cells exposed for 16 h to 2.5 μM arsenite to obtain an indication on the cellular sulphydryl status of the cells. As shown in Fig. 1D, this treatment significantly enhanced the total thiol content of the cells, with hardly any effect detected on protein thiols. In fact, the increased thiol response was entirely attributable to the non-protein thiol pool (95% of which is represented by GSH, (Meister and Anderson, 1983)).

These results indicate that, under the conditions employed, arsenite promotes time-dependent Nrf2 activation and enhanced GCLC expression associated with increased GSH biosynthesis.

### *3.2. The Nrf2 signaling pathway is activated by mitochondrial superoxide.*

DHR is a general fluorescence probe responsive to extramitochondrial $O_2^{\cdot-}$, hydrogen peroxide (Gomes et al., 2005) as well as reactive nitrogen species (Kooy et al., 1994), which

however are not produced under the experimental conditions employed in these studies (Guidarelli et al., 2016a). Fig. 2A shows the time-dependence of the DHR-fluorescence response induced by 2.5 μM arsenite that, based on the sensitivity to rotenone, AA or the respiration-deficient phenotype appears entirely mediated by mito$O_2^{\cdot-}$ (Fig. 2A). These results are in keeping with our previous findings obtained in cells exposed to arsenite for 16 h (Guidarelli et al., 2016a; Guidarelli et al., 2017). Rotenone, or AA, also suppressed the enhanced expression of both Nrf2 and GCLC (Fig. 2B), and the increased GSH biosynthesis (Fig. 2C), detected respectively 6 and 8 h after addition of 2.5 μM arsenite. In addition, the metalloid produced hardly any effect on RD cell GSH (Fig. 2C), thereby implying the absence of an upstream Nrf2 signaling in cells unable to generate mito$O_2^{\cdot-}$ in response to arsenite (Fig. 2A).

These results indicate that mito$O_2^{\cdot-}$ is the species responsible for the arsenite-dependent activation of the Nrf2/GCLC signaling leading to increased GSH biosynthesis. Complete suppression of this signaling response by treatments/manipulations abolishing mito$O_2^{\cdot-}$ formation argues against the involvement of additional mechanisms leading to activation of the transcription factor.

*3.3. The increased GSH biosynthesis reduces mitochondrial superoxide formation.*

We tested the impact of enhanced GSH synthesis in arsenite toxicity with the use of a low concentration of BSO, an inhibitor of γ-GCS (Meister and Anderson, 1983). As indicated in Fig. 3A, 2.5 μM BSO promoted a time-dependent decrease in cellular GSH, detectable after 4 h and reaching an about 30% decrease at 16 h. It was interesting to observe that a superimposable curve was obtained using cells supplemented with both BSO and arsenite, thereby implying that BSO prevents the enhanced GSH biosynthesis induced by the metalloid. The results illustrated in Fig. 3B indicate that BSO, under the same conditions, significantly increased the extent of the time-dependent DHR-fluorescence response elicited by arsenite. BSO instead failed to produce effects in the absence of additional treatments. The DHR-fluorescence response detected 8 and 16 h after addition of arsenite was suppressed by rotenone, the respiration-deficient phenotype or AA, regardless of whether induced by the metalloid alone (Fig. 2A) or associated with BSO (Fig. 3C).

These results suggest that inhibition of the GSH response significantly enhances the mitochondrial mechanisms leading to $O_2^{\cdot -}$ formation, with no evidence for a recruitment of additional mechanisms. The possibility of an activation of NADPH oxidase was nevertheless tested. We recently demonstrated that Apo and DPI, two different NADPH inhibitors (Brandes et al., 2014), fail to affect the DHR-fluorescence response evoked by arsenite in the absence of other treatments (Guidarelli et al., 2016b). The results illustrated in Fig. 3C indicate that similar results are obtained after combined exposure to arsenite and BSO. Moreover, there was no evidence of activation of NADPH oxidase, as measured by immunocytochemical detection of its membrane translocation, in cells exposed for 16 h to arsenite alone, as we previously demonstrated (Guidarelli et al., 2016b), or associated with BSO (Fig. 3Da and b). PMA was used as positive control to promote Apo-, or DPI-, sensitive activation of NADPH oxidase (Fig. 3Dc-e) and DHR fluorescence (Fig. 3Df). The results presented in this section indicate that the increased GSH biosynthesis induced by arsenite is functionally-linked to events limiting mito$O_2^{\cdot -}$ formation.

*3.4. The increased GSH biosynthesis mitigates mitochondrial dysfunction.*

We have previously reported that arsenite causes U937 cell death *via* a mechanism mediated by the formation of mito$O_2^{\cdot -}$, leading to loss of mitochondrial membrane potential and MPT, and to the ensuing triggering of the mitochondrial pathway of apoptosis (Guidarelli et al., 2015; Guidarelli et al., 2016a). We therefore tested whether BSO, by anticipating and increasing the rate of $O_2^{\cdot -}$ formation, also promotes similar effects on the apoptotic cascade. As indicated in Fig. 4A, arsenite elicited a time-dependent mitochondrial depolarization and this response was significantly increased by concomitant exposure to BSO. Furthermore, loss of mitochondrial membrane potential detected at 16 h was sensitive to treatments preventing mito$O_2^{\cdot -}$ formation and to the MPT inhibitor CsA, regardless of whether induced by the metalloid alone (Guidarelli et al., 2015; Guidarelli et al., 2016a) or associated with BSO (Fig. 4B). These results therefore suggest that BSO increases the sensitivity of the cells to MPT induced by arsenite. The CsA-sensitive release of cytochrome c was next assessed to further support the notion that the GSH response delays and

mitigates the onset of MPT in cells exposed to arsenite. For this purpose, we employed an immunocytochemical approach allowing detection of a punctuate fluorescence in untreated cells, consistently with the mitochondrial localization of cytochrome c. MPT is associated with a loss of the punctuate fluorescence as a consequence of the dilution of cytochrome c released by the mitochondria in the cytosol. The use of this approach allowed us to calculate the number of cells presenting evidence of mitochondrial loss of cytochrome c, indicative of MPT, in response to various treatments and conditions. The results summarized in Fig. 4C indicate that a 6 h exposure to arsenite promotes cytochrome c release in a very small proportion of the cells, that dramatically increased upon supplementation of BSO, which instead failed to produce effects in the absence of the metalloid. As previously observed in experiments measuring loss of mitochondrial membrane potential, the effects mediated by arsenite/BSO in terms of mitochondrial loss of cytochrome c were sensitive to CsA, rotenone, the respiration-deficient phenotype or AA. These results therefore emphasize the relevance of the GSH response elicited by arsenite in the triggering of events leading to prevention of mitochondrial dysfunction. Inhibition of *de novo* GSH biosynthesis indeed anticipates and increases mitochondrial depolarization and MPT.

*3.5. The increased GSH biosynthesis delays and mitigates apoptosis.*

We performed experiments to determine whether the increased rate of mito$O_2^{-\cdot}$ formation, resulting from inhibition of the GSH response, also anticipates and increases the arsenite-dependent apoptosis. In these experiments, the cells were exposed for 6 or 16 h to arsenite, conditions respectively associated with no or barely detectable levels of caspase 3 activation (Fig. 5A). As previously reported, significant activation of caspase 3 is instead detected after 16-48 h (Guidarelli et al., 2017). Supplementation of BSO resulted in remarkably increased caspase 3 activity, appreciable even at the shortest time of incubation. Furthermore, under both conditions, activation of caspase 3 was sensitive to CsA, rotenone, the respiration-deficient phenotype or AA. These results therefore provide evidence for a significant anticipation of the processes leading to activation of caspase 3, critically involved in the mitochondrial pathway of apoptosis (Kurokawa

and Kornbluth, 2009; Fiandalo and Kyprianou, 2012). Further analyses measuring chromatin condensation/fragmentation indeed revealed that 2.5 μM arsenite promotes an apoptotic response, barely detectable at 24 h and increasing thereafter (Fig. 5B). About 15% of the cells were apoptotic at 48 h, as we also recently reported (Guidarelli et al., 2015; Guidarelli et al., 2016a). Interestingly, BSO significantly enhanced, and remarkably anticipated, the apoptotic response mediated by the metalloid. CsA, rotenone, the respiration-deficient phenotype and AA prevented apoptosis in cells exposed to the metalloid alone (Guidarelli et al., 2016a; Guidarelli et al., 2016b) or associated with BSO (inset to Fig. 5B). The last series of experiments was performed using cells exposed for 16 h to arsenite in the absence or presence of increasing concentrations of BSO. In keeping with the results illustrated in Fig. 3A, an identical progressive decline in cellular GSH levels was observed under both conditions (Fig. 5C). Furthermore, BSO caused a dose-dependent induction of apoptosis in cells supplemented with arsenite, with hardly any effect detected after exposure to the metalloid or BSO alone (Fig. 5D). These results provide compelling evidence for the relevance of the GSH response, elicited by arsenite *via* a mechanism entirely mediated by mito$O_2^{-\cdot}$, in the triggering of events counteracting excessive mito$O_2^{-\cdot}$ formation and the ensuing mitochondrial dysfunction and apoptosis.

## 4. Discussion

Our previous studies showed that arsenite exposure of U937 cells leads to the selective and unique formation of $mitoO_2^{-\cdot}$ (Guidarelli et al., 2016a; Guidarelli et al., 2016b; Guidarelli et al., 2017), an event responsible for the triggering of downstream events leading to mitochondrial dysfunction and apoptosis (Guidarelli et al., 2016a; Guidarelli et al., 2016b). This cause-effect relationship was not established with the use of high concentrations of non-specific antioxidants/radical scavengers but, rather, with the use of treatment/manipulations selectively blunting $mitoO_2^{-\cdot}$ formation. In particular, the formation of this species was inhibited either chemically, i.e. with rotenone through the suppression of complex I activity (Degli Esposti, 1998), or with the use of cells manipulated to induce respiratory-chain deficiency. Under these different conditions, prevention of $mitoO_2^{-\cdot}$ formation was invariably associated with suppression of mitochondrial dysfunction and cytotoxicity. An additional approach to reach the same conclusion was based on the observation that pre-exposure to a low concentration of AA (10 μM) results in the same protective effects. It is important to emphasize that our previous studies demonstrated that mitochondrial AA effectively and rapidly scavenge $mitoO_2^{-\cdot}$ generated in response to arsenite (Guidarelli et al., 2015; Guidarelli et al., 2016a), with hardly any effect mediated by cytosolic AA.

This premise, while recapitulating critical information relevant for the experimental design of the present study, emphasises the notion that $mitoO_2^{-\cdot}$ is a critical player of the arsenite-dependent apoptotic response under investigation. Our results are indicative of a very little -if any- contribution of other mechanisms, for example related to the direct binding of the metalloid to protein and non-protein thiols (Shen et al., 2013; Watanabe and Hirano, 2013).

The first question addressed concerns the role of this species, and its downstream products, in the triggering of the Nrf2 cytoprotective signalling. We therefore used the same approach outlined above, however introducing a focus on the timing of the events under investigation. We initially showed that the time-dependence of Nrf2 activation is compatible with the kinetics of $mitoO_2^{-\cdot}$ formation. A cause-effect relationship between these events was then established with the

420 demonstration that Nrf2 expression is abolished by treatment/conditions suppressing mito$O_2^{-\cdot}$
421 formation.

422 It is very well known that Nrf2 activation is associated with the expression of various
423 cytoprotective genes (Abdul-Aziz et al., 2015; Tebay et al., 2015; Hourihan et al., 2016). We
424 focused our attention on GCLC and found that its time-dependent increased expression, and the
425 resulting enhanced GSH biosynthesis, were also kinetically compatible with the upstream role of
426 mito$O_2^{-\cdot}$ and the ensuing Nrf2 activation. Not surprisingly, treatments blunting Nrf2 activation
427 through inhibition of mito$O_2^{-\cdot}$ formation also abolished the increased GCLC expression and GSH
428 biosynthesis.

429 The results thus far discussed allow a first conclusion, possibly relevant in different cellular
430 systems in which arsenite selectively promotes the formation of mito$O_2^{-\cdot}$. This species cannot exit
431 mitochondria and is in fact rapidly dismutated by MnSOD to diffusible $H_2O_2$ (Hamanaka and
432 Chandel, 2010; Kudryavtseva et al., 2016). In this direction we recently showed that, under the
433 same conditions employed in this study, arsenite-derived $H_2O_2$ produces distal effects, as DNA
434 strand scissions and modulation of gene expression (Guidarelli et al., 2017). Hence, the above
435 results are consistent with the notion that mito$O_2^{-\cdot}$, *via* the resulting $H_2O_2$, is the only species
436 involved in Nrf2 expression/activation, and in the ensuing GSH response. This consideration
437 apparently rules out the possible contribution of other mechanisms, as the direct binding of arsenic
438 to Nrf2 itself, or Keap1, previously described in other systems, in which however the source of the
439 radical species produced were not determined (He and Ma, 2009; He and Ma, 2010; Lau et al.,
440 2013).

441 A more general conclusion from our results is instead that mito$O_2^{-\cdot}$ plays a pivotal role in the
442 response of the cells to arsenite, as it critically regulates the triggering of both toxicity and
443 cytoprotective mechanisms. Future studies should determine whether the same is true for
444 NADPH-oxidase derived $O_2^{-\cdot}$ and whether the same relationship is eventually maintained under
445 conditions in which both mechanisms are sequentially recruited. This notion will be addressed in

446 the respiration-deficient cells used in this study, that require about 4 time greater concentrations of
447 arsenite to significantly activate NADPH oxidase (Guidarelli *et al.*, 2016b).

448 An additional consideration we can make is on the relationships existing between the rate of
449 mito$O_2^{-\cdot}$/$H_2O_2$ formation and the increased GSH biosynthesis. It has been proposed that binding of
450 arsenic to GSH leads to formation of a conjugate extruded by the cells *via* multidrug transporters,
451 an event resulting in GSH depletion and enforcing ROS formation (Leslie, 2012; Watanabe and
452 Hirano, 2013). Although the formation of the arsenic/GSH complex, and the consequent decline
453 in GSH content, would be masked by the enhanced GSH biosynthesis, we nevertheless consider
454 poorly relevant its occurrence in the toxicity paradigm under investigation, since the GSH levels
455 observed after inhibition of mito$O_2^{-\cdot}$ formation were identical to those detected in untreated cells.
456 Our conclusion is therefore that mito$O_2^{-\cdot}$/$H_2O_2$ formation is not the consequence of GSH depletion
457 but rather a cause, eventually concealed by the Nrf2 signalling response. Another point we can
458 make is that, in the toxicity paradigm under investigation, the contribution of detoxification
459 mechanisms based on the formation of GSH-trivalent arsenic complexes (Leslie, 2012; Watanabe
460 and Hirano, 2013) is poor, or negligible.

461 The second major question addressed was on the significance of the Nrf2/GCLC/GSH
462 response, under the same conditions in which the metalloid triggers these events, and the
463 mitochondrial pathway of apoptosis, in response to the same mito$O_2^{-\cdot}$-dependent signalling. This
464 question cannot find an explanation on previous findings obtained using cells with down-regulated
465 Nrf2 (or GCLC) expression, as obtained using siRNA technologies or KO mice (Jiang et al., 2009;
466 Yang et al., 2012; Yang et al., 2015), or using approaches (e.g., BSO prior to treatment with
467 arsenite) leading to an initial decreased GSH pool (Meister and Anderson, 1983). All these
468 conditions are indeed associated with an impaired defence machinery and with an acquired
469 susceptibility to arsenite toxicity, which can obviously become apparent regardless of the source
470 of ROS involved.

471 The question we asked is more specifically linked to the condition of acute arsenite exposure
472 associated with the ongoing toxicity and protective signalling pathway triggered by mito$O_2^{-\cdot}$. Our
473 kinetic studies established that the Nrf2/GCLC/GSH pathway is characterised by a rapid
474 occurrence, as maximally activated within the first 6-8 h of exposure to the metalloid.
475 Mitochondrial dysfunction is also detected under the same conditions, but then further increases in
476 the subsequent 8 h to finally promote delayed apoptotic DNA fragmentation, detected after 48 h in
477 about 15% of the cells. We were interested to determine the specific impact of the
478 Nrf2/GCLC/GSH pathway in the timing/extent of the above responses.

479 In order to approach this issue, we first established that a low concentration of BSO, 2.5 μM,
480 suppresses the GSH response to then demonstrate that this manipulation significantly increased
481 the rate of ROS formation induced by arsenite. Interestingly, this event was entirely mediated by
482 the increased mito$O_2^{-\cdot}$ formation, since completely suppressed by rotenone, the respiration-
483 deficient phenotype or AA. In addition, we also ruled out the possibility of a recruitment of other
484 mechanisms leading to $O_2^{-\cdot}$ formation, as the activation of NADPH oxidase.

485 These results therefore suggest that the triggering of the GSH response mitigates the extent of
486 time-dependent mito$O_2^{-\cdot}$ release. Although more studies should specifically address this issue, it
487 appears that mito$O_2^{-\cdot}$ initially produced by arsenite triggers the GSH response to down-modulate
488 further mito$O_2^{-\cdot}$ release. In this perspective, the increased GSH biosynthesis, which only takes
489 place in the cytosol, should lead to increased mitochondrial accumulation of GSH, an established
490 and well-characterised process (Ribas et al., 2014; Calabrese et al., 2017). Mitochondrial GSH
491 would then promote its effects by reducing mito$O_2^{-\cdot}$ formation in the mitochondrial respiratory
492 chain and supporting reactions leading to prevention of mitochondrial damage or to detoxification
493 of $H_2O_2$ (Ribas et al., 2014; Calabrese et al., 2017).

494 A final observation from this study was that the increased rate of mito$O_2^{-\cdot}$ formation
495 associated with prevention of the GSH response is followed by a dramatic anticipation of
496 mitochondrial dysfunction and downstream events leading to apoptosis.

In conclusion, our results indicate that a low concentration of arsenite induces in U937 cells a time-dependent mito$O_2^{-\cdot}$ formation leading to delayed MPT-dependent apoptosis. Under the same treatment conditions, mito$O_2^{-\cdot}$-derived $H_2O_2$ diffuses to extramitochondrial compartments, thereby promoting early activation of the Nrf2/GCLC/GSH signalling. Enhanced GSH biosynthesis is then associated with inhibition of excessive mito$O_2^{-\cdot}$ formation, with an ensuing decreased and delayed mitochondrial dysfunction and apoptosis. Suppression of this signalling is indeed invariably associated with remarkably accelerated and enhanced rates of events leading to MPT-dependent apoptosis.

## Conflict of interest statement

There are no conflicts of interest.

## Transparency Document

The transparency document associated with this article can be found in the online submission.


## Funding

This work was supported by Ministero dell'Università e della Ricerca Scientifica e Tecnologica, Programmi di Ricerca Scientifica di Rilevante Interesse Nazionale, 2015, [Grant number: 2015MJBEM2-003. O.C.].

519 **References**
520
521 Abdul-Aziz, A., MacEwan, D.J., Bowles, K.M., Rushworth, S.A., 2015. Oxidative stress
522 responses and NRF2 in human leukaemia. Oxid. Med. Cell. Longev. 2015, 454659.
523 Azzolini, C., Fiorani, M., Cerioni, L., Guidarelli, A., Cantoni, O., 2013. Sodium-dependent
524 transport of ascorbic acid in U937 cell mitochondria. IUBMB Life 65, 149-153.
525 Beutler, E., 1984. Red cell metabolism: a manual of biochemical methods. Grune & Stratton, New
526 York.
527 Brand, K.A., Hermfisse, U., 1997. Aerobic glycolysis by proliferating cells: a protective strategy
528 against reactive oxygen species. FASEB J. 11, 388-395.
529 Brandes, R.P., Weissmann, N., Schroder, K., 2014. Nox family NADPH oxidases: Molecular
530 mechanisms of activation. Free Radic. Biol. Med. 76, 208-226.
531 Brundu, S., Palma, L., Picceri, G.G., Ligi, D., Orlandi, C., Galluzzi, L., Chiarantini, L.,
532 Casabianca, A., Schiavano, G.F., Santi, M., Mannello, F., Green, K., Smietana, M.,
533 Magnani, M., Fraternale, A., 2016. Glutathione Depletion Is Linked with Th2 Polarization
534 in Mice with a Retrovirus-Induced Immunodeficiency Syndrome, Murine AIDS: Role of
535 Proglutathione Molecules as Immunotherapeutics. J. Virol. 90, 7118-7130.
536 Calabrese, G., Morgan, B., Riemer, J., 2017. Mitochondrial Glutathione: Regulation and
537 Functions. Antioxid. Redox. Signal. 27, 1162-1177.
538 Chen, C., Jiang, X., Gu, S., Lai, Y., Liu, Y., Zhang, Z., 2017. Protection of Nrf2 against arsenite-
539 induced oxidative damage is regulated by the cyclic guanosine monophosphate-protein
540 kinase G signaling pathway. Environ. Toxicol. 32, 2004-2020.
541 Choudhury, S., Ghosh, S., Mukherjee, S., Gupta, P., Bhattacharya, S., Adhikary, A.,
542 Chattopadhyay, S., 2016. Pomegranate protects against arsenic-induced p53-dependent
543 ROS-mediated inflammation and apoptosis in liver cells. J. Nutr. Biochem. 38, 25-40.
544 Degli Esposti, M., 1998. Inhibitors of NADH-ubiquinone reductase: an overview. Biochim.
545 Biophys. Acta 1364, 222-235.

546 Ellinsworth, D.C., 2015. Arsenic, reactive oxygen, and endothelial dysfunction. J. Pharmacol.
547 Exp. Ther. 353, 458-464.
548 Ellman, G.L., 1959. Tissue sulfhydryl groups. Arch. Biochem. Biophys. 82, 70-77.
549 Fiandalo, M.V., Kyprianou, N., 2012. Caspase control: protagonists of cancer cell apoptosis. Exp.
550 Oncol. 34, 165-175.
551 Fiorani, M., Azzolini, C., Cerioni, L., Scotti, M., Guidarelli, A., Ciacci, C., Cantoni, O., 2015a.
552 The mitochondrial transporter of ascorbic acid functions with high affinity in the presence
553 of low millimolar concentrations of sodium and in the absence of calcium and magnesium.
554 Biochim. Biophys. Acta 1848, 1393-1401.
555 Fiorani, M., Azzolini, C., Guidarelli, A., Cerioni, L., Scotti, M., Cantoni, O., 2015b. Intracellular
556 dehydroascorbic acid inhibits SVCT2-dependent transport of ascorbic acid in
557 mitochondria. Pharmacol. Res. 99, 289-295.
558 Flora, S.J., 2011. Arsenic-induced oxidative stress and its reversibility. Free Radic. Biol. Med. 51,
559 257-281.
560 Forman, H.J., 2016. Redox signaling: An evolution from free radicals to aging. Free Radic. Biol.
561 Med. 97, 398-407.
562 Franklin, C.C., Backos, D.S., Mohar, I., White, C.C., Forman, H.J., Kavanagh, T.J., 2009.
563 Structure, function, and post-translational regulation of the catalytic and modifier subunits
564 of glutamate cysteine ligase. Mol. Aspects Med. 30, 86-98.
565 Gomes, A., Fernandes, E., Lima, J.L., 2005. Fluorescence probes used for detection of reactive
566 oxygen species. J. Biochem. Biophys. Methods 65, 45-80.
567 Gong, X., Ivanov, V.N., Hei, T.K., 2016. 2,3,5,6-Tetramethylpyrazine (TMP) down-regulated
568 arsenic-induced heme oxygenase-1 and ARS2 expression by inhibiting Nrf2, NF-kappaB,
569 AP-1 and MAPK pathways in human proximal tubular cells. Arch. Toxicol. 90, 2187-
570 2200.

571 Griffith, O.W., Mulcahy, R.T., 1999. The enzymes of glutathione synthesis: gamma-
572 glutamylcysteine synthetase. Adv. Enzymol. Relat. Areas Mol. Biol. 73, 209-267.
573 Guidarelli, A., Carloni, S., Balduini, W., Fiorani, M., Cantoni, O., 2016a. Mitochondrial ascorbic
574 acid prevents mitochondrial $O_2^{\cdot-}$ formation, an event critical for U937 cell apoptosis
575 induced by arsenite through both autophagic-dependent and independent mechanisms.
576 Biofactors 42, 190-200.
577 Guidarelli, A., Cerioni, L., Tommasini, I., Fiorani, M., Brune, B., Cantoni, O., 2005. Role of Bcl-2
578 in the arachidonate-mediated survival signaling preventing mitochondrial permeability
579 transition-dependent U937 cell necrosis induced by peroxynitrite. Free Radic. Biol. Med.
580 39, 1638-1649.
581 Guidarelli, A., Fiorani, M., Azzolini, C., Cerioni, L., Scotti, M., Cantoni, O., 2015. U937 cell
582 apoptosis induced by arsenite is prevented by low concentrations of mitochondrial ascorbic
583 acid with hardly any effect mediated by the cytosolic fraction of the vitamin. Biofactors
584 41, 101-110.
585 Guidarelli, A., Fiorani, M., Carloni, S., Cerioni, L., Balduini, W., Cantoni, O., 2016b. The study of
586 the mechanism of arsenite toxicity in respiration-deficient cells reveals that NADPH
587 oxidase-derived superoxide promotes the same downstream events mediated by
588 mitochondrial superoxide in respiration-proficient cells. Toxicol. Appl. Pharmacol. 307,
589 35-44.
590 Guidarelli, A., Fiorani, M., Cerioni, L., Scotti, M., Cantoni, O., 2017. Arsenite induces DNA
591 damage via mitochondrial ROS and induction of mitochondrial permeability transition.
592 Biofactors 43, 673-684.
593 Hamanaka, R.B., Chandel, N.S., 2010. Mitochondrial reactive oxygen species regulate cellular
594 signaling and dictate biological outcomes. Trends Biochem. Sci. 35, 505-513.

595 He, X., Ma, Q., 2009. NRF2 cysteine residues are critical for oxidant/electrophile-sensing, Kelch-
596 like ECH-associated protein-1-dependent ubiquitination-proteasomal degradation, and
597 transcription activation. Mol. Pharmacol. 76, 1265-1278.
598 He, X., Ma, Q., 2010. Critical cysteine residues of Kelch-like ECH-associated protein 1 in arsenic
599 sensing and suppression of nuclear factor erythroid 2-related factor 2. J. Pharmacol. Exp.
600 Ther. 332, 66-75.
601 Hou, Y., Wang, Y., Wang, H., Xu, Y., 2014. Induction of glutathione synthesis in human
602 hepatocytes by acute and chronic arsenic exposure: differential roles of mitogen-activated
603 protein kinases. Toxicology 325, 96-106.
604 Hourihan, J.M., Moronetti Mazzeo, L.E., Fernandez-Cardenas, L.P., Blackwell, T.K., 2016.
605 Cysteine Sulfenylation Directs IRE-1 to Activate the SKN-1/Nrf2 Antioxidant Response.
606 Mol. Cell. 63, 553-566.
607 Jiang, T., Huang, Z., Chan, J.Y., Zhang, D.D., 2009. Nrf2 protects against As(III)-induced damage
608 in mouse liver and bladder. Toxicol. Appl. Pharmacol. 240, 8-14.
609 Jomova, K., Jenisova, Z., Feszterova, M., Baros, S., Liska, J., Hudecova, D., Rhodes, C.J., Valko,
610 M., 2011. Arsenic: toxicity, oxidative stress and human disease. J. Appl. Toxicol. 31, 95-
611 107.
612 Kooy, N.W., Royall, J.A., Ischiropoulos, H., Beckman, J.S., 1994. Peroxynitrite-mediated
613 oxidation of dihydrorhodamine 123. Free Radic. Biol. Med. 16, 149-156.
614 Kudryavtseva, A.V., Krasnov, G.S., Dmitriev, A.A., Alekseev, B.Y., Kardymon, O.L.,
615 Sadritdinova, A.F., Fedorova, M.S., Pokrovsky, A.V., Melnikova, N.V., Kaprin, A.D.,
616 Moskalev, A.A., Snezhkina, A.V., 2016. Mitochondrial dysfunction and oxidative stress in
617 aging and cancer. Oncotarget 7, 44879-44905.
618 Kurokawa, M., Kornbluth, S., 2009. Caspases and kinases in a death grip. Cell 138, 838-854.
619 Lau, A., Whitman, S.A., Jaramillo, M.C., Zhang, D.D., 2013. Arsenic-mediated activation of the
620 Nrf2-Keap1 antioxidant pathway. J. Biochem. Mol. Toxicol. 27, 99-105.

621 Leslie, E.M., 2012. Arsenic-glutathione conjugate transport by the human multidrug resistance
622 proteins (MRPs/ABCCs). J. Inorg. Biochem. 108, 141-149.
623 Li, B., Li, X., Zhu, B., Zhang, X., Wang, Y., Xu, Y., Wang, H., Hou, Y., Zheng, Q., Sun, G.,
624 2013. Sodium arsenite induced reactive oxygen species generation, nuclear factor
625 (erythroid-2 related) factor 2 activation, heme oxygenase-1 expression, and glutathione
626 elevation in Chang human hepatocytes. Environ. Toxicol. 28, 401-410.
627 Li, Y.N., Xi, M.M., Guo, Y., Hai, C.X., Yang, W.L., Qin, X.J., 2014. NADPH oxidase-
628 mitochondria axis-derived ROS mediate arsenite-induced HIF-1alpha stabilization by
629 inhibiting prolyl hydroxylases activity. Toxicol. Lett. 224, 165-174.
630 Liu, S.X., Davidson, M.M., Tang, X., Walker, W.F., Athar, M., Ivanov, V., Hei, T.K., 2005.
631 Mitochondrial damage mediates genotoxicity of arsenic in mammalian cells. Cancer Res.
632 65, 3236-3242.
633 Lowry, O.H., Rosebrough, N.J., Farr, A.L., Randall, R.J., 1951. Protein measurement with the
634 Folin phenol reagent. J. Biol. Chem. 193, 265-275.
635 Mandal, P., 2017. Molecular insight of arsenic-induced carcinogenesis and its prevention. Naunyn
636 Schmiedebergs Arch. Pharmacol. 390, 443-455.
637 Meister, A., Anderson, M.E., 1983. Glutathione. Annu. Rev. Biochem. 52, 711-760.
638 Pi, J., Qu, W., Reece, J.M., Kumagai, Y., Waalkes, M.P., 2003. Transcription factor Nrf2
639 activation by inorganic arsenic in cultured keratinocytes: involvement of hydrogen
640 peroxide. Exp. Cell Res. 290, 234-245.
641 Rao, C.V., Pal, S., Mohammed, A., Farooqui, M., Doescher, M.P., Asch, A.S., Yamada, H.Y.,
642 2017. Biological effects and epidemiological consequences of arsenic exposure, and
643 reagents that can ameliorate arsenic damage in vivo. Oncotarget 8, 57605-57621.
644 Ray, P.D., Huang, B.W., Tsuji, Y., 2015. Coordinated regulation of Nrf2 and histone H3 serine 10
645 phosphorylation in arsenite-activated transcription of the human heme oxygenase-1 gene.
646 Biochim. Biophys. Acta 1849, 1277-1288.

Ribas, V., Garcia-Ruiz, C., Fernandez-Checa, J.C., 2014. Glutathione and mitochondria. Front. Pharmacol. 5, 151.

Rossler, O.G., Thiel, G., 2017. Specificity of Stress-Responsive Transcription Factors Nrf2, ATF4, and AP-1. J. Cell. Biochem. 118, 127-140.

Shen, S., Li, X.F., Cullen, W.R., Weinfeld, M., Le, X.C., 2013. Arsenic binding to proteins. Chem. Rev. 113, 7769-7792.

Smith, K.R., Klei, L.R., Barchowsky, A., 2001. Arsenite stimulates plasma membrane NADPH oxidase in vascular endothelial cells. Am. J. Physiol. Lung Cell. Mol. Physiol. 280, L442-449.

Son, Y.O., Pratheeshkumar, P., Roy, R.V., Hitron, J.A., Wang, L., Divya, S.P., Xu, M., Luo, J., Chen, G., Zhang, Z., Shi, X., 2015. Antioncogenic and Oncogenic Properties of Nrf2 in Arsenic-induced Carcinogenesis. J. Biol. Chem. 290, 27090-27100.

Straub, A.C., Clark, K.A., Ross, M.A., Chandra, A.G., Li, S., Gao, X., Pagano, P.J., Stolz, D.B., Barchowsky, A., 2008. Arsenic-stimulated liver sinusoidal capillarization in mice requires NADPH oxidase-generated superoxide. J. Clin. Invest. 118, 3980-3989.

Tebay, L.E., Robertson, H., Durant, S.T., Vitale, S.R., Penning, T.M., Dinkova-Kostova, A.T., Hayes, J.D., 2015. Mechanisms of activation of the transcription factor Nrf2 by redox stressors, nutrient cues, and energy status and the pathways through which it attenuates degenerative disease. Free Radic. Biol. Med. 88, 108-146.

Wang, X.J., Sun, Z., Chen, W., Eblin, K.E., Gandolfi, J.A., Zhang, D.D., 2007. Nrf2 protects human bladder urothelial cells from arsenite and monomethylarsonous acid toxicity. Toxicol. Appl. Pharmacol. 225, 206-213.

Watanabe, T., Hirano, S., 2013. Metabolism of arsenic and its toxicological relevance. Arch. Toxicol. 87, 969-979.

Yang, B., Fu, J., Zheng, H., Xue, P., Yarborough, K., Woods, C.G., Hou, Y., Zhang, Q., Andersen, M.E., Pi, J., 2012. Deficiency in the nuclear factor E2-related factor 2 renders

673 pancreatic beta-cells vulnerable to arsenic-induced cell damage. Toxicol. Appl. Pharmacol.
674 264, 315-323.
675 Yang, X., Wang, D., Ma, Y., Xu, X., Zhu, Z., Wang, X., Deng, H., Li, C., Chen, M., Tong, J.,
676 Yamanaka, K., An, Y., 2015. Continuous activation of Nrf2 and its target antioxidant
677 enzymes leads to arsenite-induced malignant transformation of human bronchial epithelial
678 cells. Toxicol. Appl. Pharmacol. 289, 231-239.

679
680

## Figures

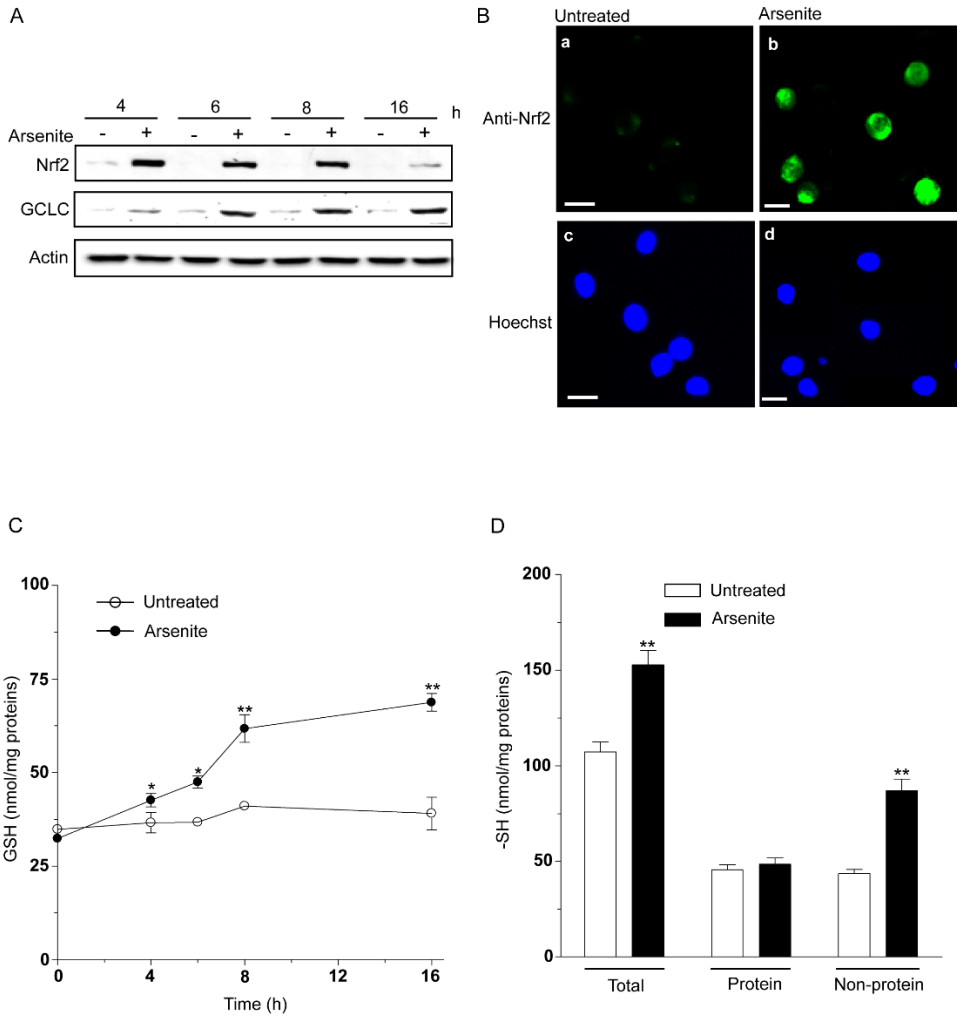


**Fig. 1.** Arsenite promotes a time-dependent expression of Nrf2 and CGLC accompanied by increased GSH biosynthesis. (A) Cells were exposed for increasing time intervals to 2.5 µM arsenite and analysed for Nrf2 and GCLC expression using actin as a loading control. (B) Representative images providing evidence of Nrf2 expression/nuclear localization in cells exposed for 6 h to arsenite. Immunofluorescence staining indicative of Nrf2 expression in cells exposed to the vehicle (a) or to arsenite (b). (c) and (d) are images taken from the same field in which the nuclear compartments are identified by Hoechst staining. Scale bar represents 20 µm. (C) Cells were exposed for increasing time-intervals to arsenite and then analysed for their GSH content by HPLC. (D) Cells exposed for 16 h to arsenite were analysed for their total, protein and non protein thiol content, as detailed under Materials and methods. Results represent the means ± SD calculated from at least 3 separate experiments. *P < 0.05, **P < 0.01, as compared to untreated cells (one-way ANOVA followed by Dunnet's test).

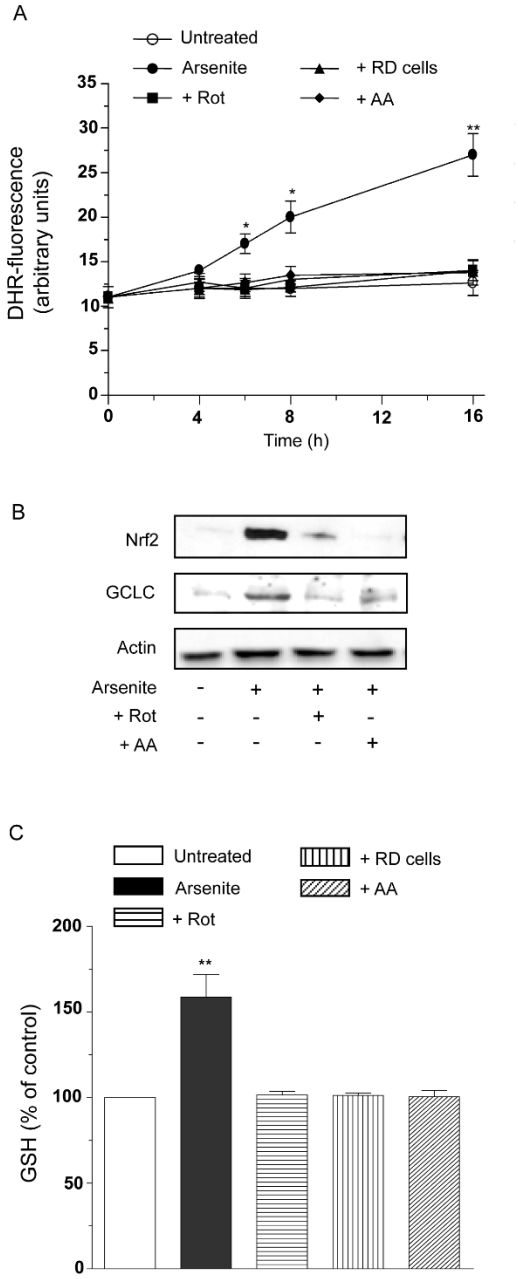


**Fig. 2.** Mitochondrial superoxide mediates the arsenite-dependent Nrf2/GCLC/GSH response. (A) Cells were exposed for increasing time intervals to 2.5 µM arsenite, either alone or associated with 0.5 µM rotenone (Rot) or 10 µM AA and analysed for their DHR-fluorescence response. The effect of arsenite was also investigated in RD cells. Results represent the means ± SD calculated from at least 3 separate experiments. *P < 0.05, **P < 0.01, as compared to untreated cells (two-way ANOVA followed by Bonferroni's test).
(B) Cells were exposed for 6h to 2.5 µM arsenite, either alone or associated with rotenone (Rot) or AA, and analysed for Nrf2 and GCLC expression.
(C) Cells were exposed for 16h to 2.5 µM arsenite, either alone or associated with rotenone (Rot) or AA, and analysed for their GSH content. The effect of arsenite was also tested in RD cells. GSH content is expressed as a percentage of the GSH concentration found in the control cells. Results represent the means ± SD calculated from at least 3 separate experiments. **P < 0.01, as compared to untreated cells (one-way ANOVA followed by Dunnet's test).

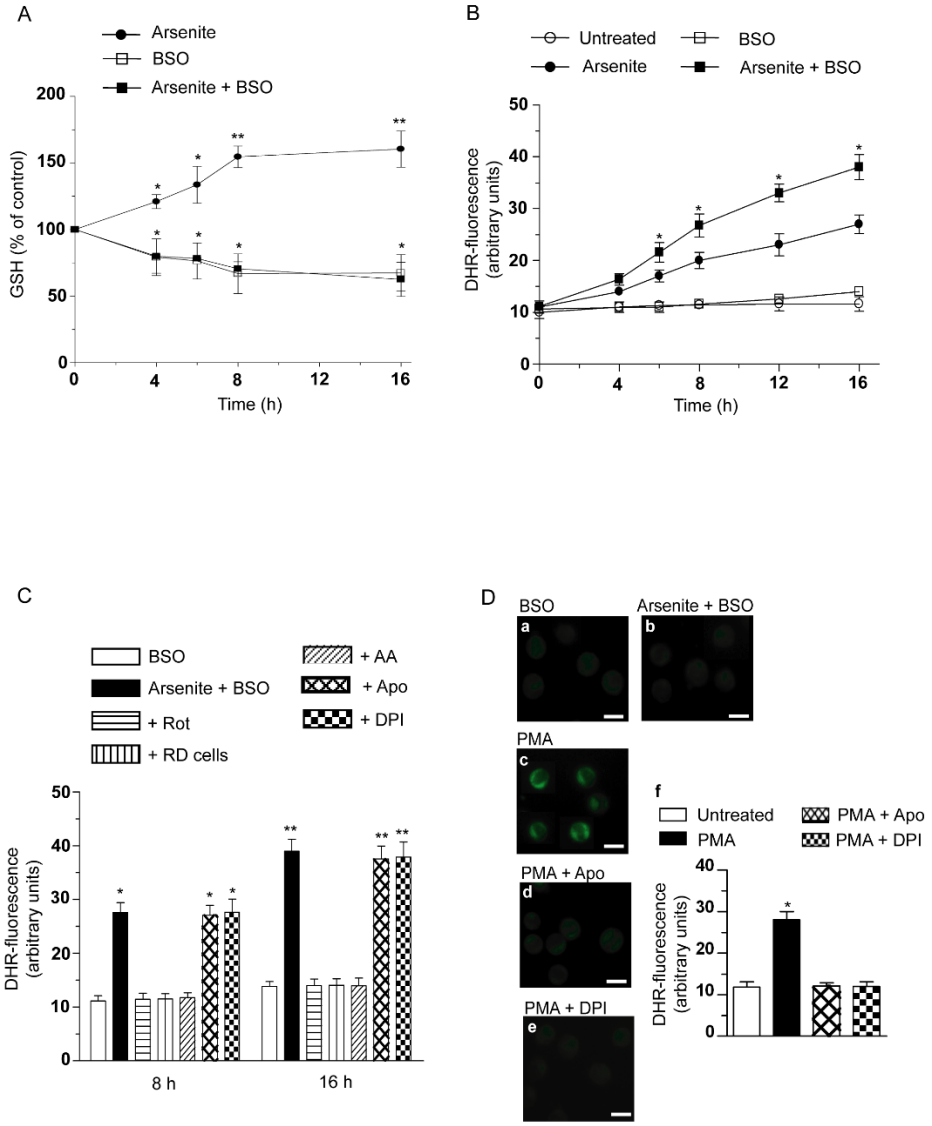


**Fig. 3.** The enhanced GSH biosynthesis reduces the rate of mitochondrial superoxide formation induced by arsenite. (A and B) Cells were exposed for increasing time intervals to 0 or 2.5 μM arsenite, both in the absence or presence of 2.5 μM BSO. At the indicated times, aliquots of the cells were processed for the measurement of their GSH content (results are expressed as a percentage of the GSH content of their appropriate controls, A) and for the analysis of the DHR-fluorescence response (B). Results represent the means ± SD calculated from at least 3 separate experiments. *P < 0.05, **P < 0.01, as compared to untreated cells or arsenite treated cells (two-way ANOVA followed by Bonferroni's test). (C) Cells were treated for 8 or 16 h with arsenite and BSO, both in the absence or presence of rotenone (Rot), AA, DPI (1 μM) or Apo (10 μM). After treatments, the cells were analyzed for DHR-fluorescence. The effect of arsenite/BSO was also tested in RD cells. (D) Representative micrographs showing p47phox localization in cells exposed for 16 h to BSO alone (a) or associated with arsenite (b). In other experiments the cells were exposed for 30 min to 100 μg/ml PMA alone (c) or associated with Apo (d), or DPI (e). The inhibitors were added to the cultures 15 min prior to PMA treatment. The micrographs are representative of at least three separate experiments. Scale bar represents 20 μm. Panel (f) shows the DHR-fluorescence response detected in cells exposed to PMA in the absence or presence of Apo, or DPI. Results represent the means ± SD calculated from at least 3 separate experiments. *P < 0.05, **P < 0.01, as compared to untreated cells (one-way ANOVA followed by Dunnet's test).

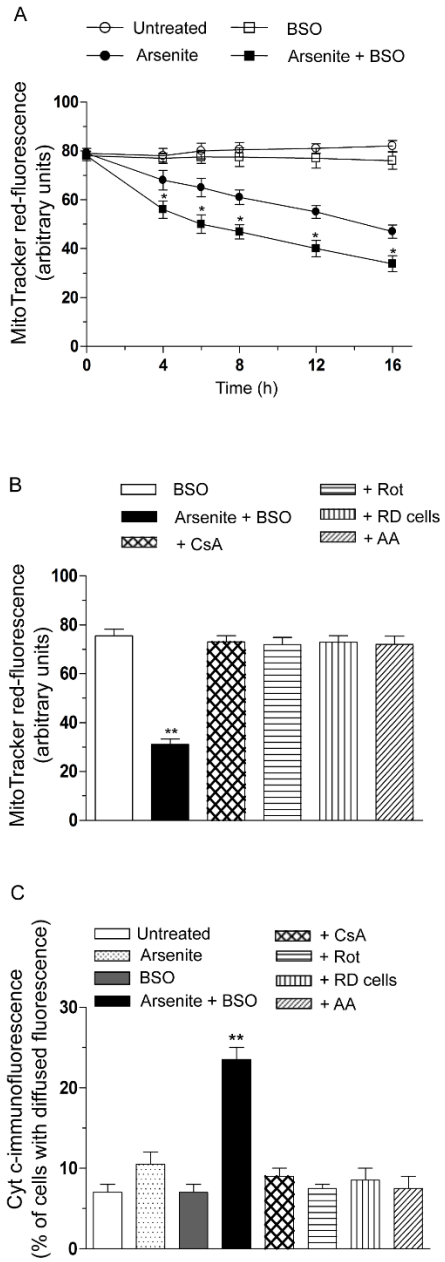


**Fig. 4.** The increased GSH biosynthesis mitigates and delays mitochondrial dysfunction induced by arsenite. (A) Cells were exposed for increasing time intervals to arsenite alone or associated with BSO. After treatments, the cells were analyzed for MitoTracker red CMXRos-fluorescence. Results represent the means ± SD calculated from at least 3 separate experiments. *P < 0.05, as compared to arsenite treated cells (two-way ANOVA followed by Bonferroni's test). (B) Cells were exposed for 16 h to arsenite and BSO in the absence or presence of rotenone (Rot), AA, or CsA (0.5 μM). Selected experiments were performed using RD cells. After treatments, the cells were analyzed for MitoTracker red CMXRos-fluorescence. Results represent the means ± SD calculated from at least 3 separate experiments. **P < 0.01, as compared to untreated cells (one-way ANOVA followed by Dunnet's test). (C) Cells were exposed for 6 h to arsenite alone, or associated with BSO, both in absence or presence of rotenone (Rot), AA, or CsA. The effect of arsenite/BSO was also tested in RD cells. After treatments, cytochrome c localization was determined by immunofluorescence staining with anti-FITC antibody. The graph shows the percentage of cells with diffused fluorescence as a consequence of the mitochondrial loss of cytochrome c (n=150). **P < 0.01, as compared to untreated cells (one-way ANOVA followed by Dunnet's test).

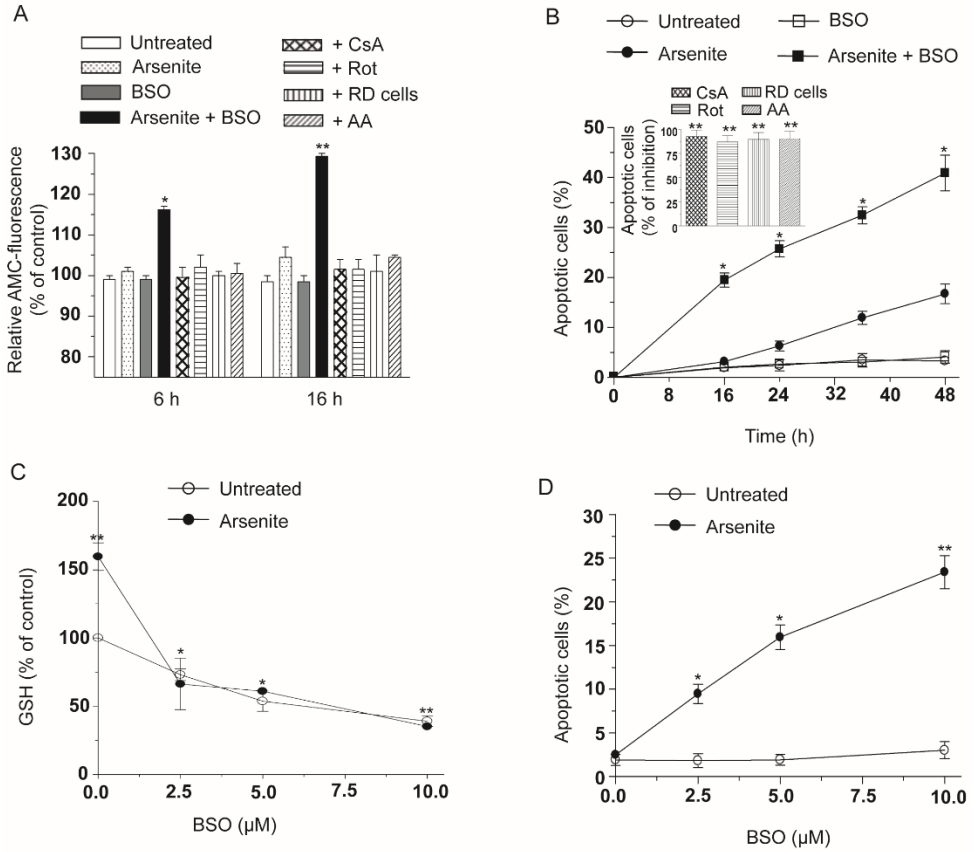


**Fig. 5.** The increased GSH biosynthesis mitigates and delays the apoptotic death induced by arsenite. (A) Cells were exposed for 6 or 16 h to arsenite alone, or associated with BSO, both in absence or presence of rotenone (Rot), AA, or CsA. The effect of arsenite/BSO was also tested in RD cells. After treatments, the cells were analysed for caspase-3 activity, as detailed in Materials and methods. Results represent the means ± SD calculated from at least 3 separate experiments. *P < 0.05, **P < 0.01, as compared to untreated cells (one-way ANOVA followed by Dunnet's test). (B) Cells were exposed for increasing time intervals to arsenite alone or associated with BSO. After treatments, the cells were analyzed for apoptosis, by measuring chromatin fragmentation/condensation with the Hoechst assay. Results represent the means ± SD calculated from at least 3 separate experiments. *P < 0.05, as compared to arsenite treated cells (two-way ANOVA followed by Bonferroni's test). The inset shows the effect of CsA, rotenone (Rot), AA or the respiration-deficient phenotype on the apoptotic response mediated by a 16 h exposure to arsenite/BSO. Results represent the means ± SD calculated from at least 3 separate experiments. **P < 0.01, as compared to cells exposed to arsenite/BSO (one-way ANOVA followed by Dunnet's test). Cells were exposed for 16 h to increasing concentrations of BSO in the absence or presence of arsenite and analysed for (C) GSH content (expressed as a percentage of the GSH concentration found in the control cells) and for (D) apoptotic DNA fragmentation/condensation. Results represent the means ± SD calculated from at least 3 separate experiments. *P < 0.05, **P < 0.01, as compared to untreated cells (two-way ANOVA followed by Bonferroni's test).